SIViP (2017) 11:589–596
DOI 10.1007/s11760-016-0998-y

ORIGINAL PAPER

Sparse representation-based algorithm for joint SAR image formation and autofocus

Mohammad Javad Hasankhan[1] · **Sadegh Samadi**[1] · **Müjdat Çetin**[2]

Received: 19 September 2015 / Revised: 8 October 2016 / Accepted: 12 October 2016 / Published online: 27 October 2016

Abstract Inaccuracies in the observation model of the synthetic aperture radar (SAR) due to inaccuracies of the velocity and position of the platform or atmospheric turbulence cause degradations in reconstructed images which necessitate the use of autofocus algorithms. In this paper we propose a novel signal processing algorithm for joint SAR image formation and autofocus in a synthesis dictionary based sparse representation framework. Proposed algorithm can be applied broadly to scenes that exhibit sparsity with respect to any dictionary. This is done by extending our previously developed sparse representation-based SAR imaging framework to joint SAR image formation and autofocus. To this end, the phase error vector is separated from the unknown phase of the complex-valued back-scattered field. Phase error vector is estimated using a MAP estimator and compensated through an iterative algorithm to produce focused images. We demonstrate the effectiveness of the proposed approach on synthetic and real imagery.

Keywords Synthetic aperture radar (SAR) · Autofocus · Sparse representation · Synthesis dictionary · Phase error

Electronic supplementary material The online version of this article (doi:10.1007/s11760-016-0998-y) contains supplementary material, which is available to authorized users.

✉ Sadegh Samadi
samadi@sutech.ac.ir

Mohammad Javad Hasankhan
m.j.hasankhan@sutech.ac.ir

Müjdat Çetin
mcetin@sabanciuniv.edu

[1] Shiraz University of Technology, Shiraz, Iran

[2] Sabanci University, Istanbul, Turkey

1 Introduction

Synthetic aperture radar (SAR) is an active microwave sensor producing high resolution 2-D images of the ground with processing of Doppler shift in azimuth direction in addition to normal radar range processing [1]. SAR imaging problem is an inverse problem to be solved based on the mathematical model of the observation process. The observed signal directly depends on the two way propagation time from the platform to the field which is called demodulation time. Exact measurement of this time is influenced by several parameters. One of these parameters is the distance from the center of the scene to the sensor which may be inaccurate due to slip and mobility of the platform. Inexact knowledge of the demodulation time causes phase errors in SAR data, which results in defocusing of the reconstructed image [2].

In this paper, we consider the spotlight mode of SAR [2]. Conventional image formation method in spotlight mode SAR is the polar format algorithm (PFA), which is based on the two dimensional Fourier transform [2,3]. Some limiting factors of PFA are limited resolution, side-lobe artifacts, and speckle noise. In addition, the conventional PFA method has no mechanism to counter image defocusing caused by phase errors during the image formation process. There are several methods to compensate the effect of phase errors on the conventionally reconstructed images, which are referred to as autofocus methods. Phase gradient autofocus (PGA) [4] is one of the most successful and widely used autofocusing methods that estimates phase errors by windowing and center shifting on isolated defocused targets. Multichannel autofocus (MCA) is another autofocus technique that estimates 1-D phase error functions by solving a set of linear equations [5]. These autofocus techniques for estimation and compensation of phase errors are based

on post-processing of defocused images produced by conventional reconstruction methods. Recently, a nonquadratic regularization-based image reconstruction method has been proposed for SAR image formation and autofocusing simultaneously [6].

In this new method, phase errors are compensated during the image formation process and the problem is set up as an optimization problem using nonquadratic regularization method [7]. Similar ideas have been developed in [8,9] too. This new framework is quite effective in phase error estimation and compensation. However, in the formulation developed in [6], it is implicitly assumed that the image of the underlying scene is sparse. For scenes that are not sparse directly in the image domain, such as scenes with a large smooth area of strong scatterers, this method may produce a poor reconstruction. Such scenes might exhibit sparsity in a different domain, which could be captured by a dictionary.

In this paper, we extend the work in [6] for any scene that has a sparse representation in a proper dictionary and develop a new method for simultaneous SAR image formation and autofocus. This is done by extending the sparse representation-based SAR imaging method [10] for simultaneous SAR image formation and autofocusing. The approach in [10] allows the use of any overcomplete synthesis dictionary to represent the scene reflectivities.

In this framework, due to the complex-valued nature of SAR images, the phase component of the complex backscattered field should be estimated in parallel with the phase error. Throughout the paper, upper case and lower case bold face characters denote matrices and vectors, respectively.

2 The effect of phase errors on the linear SAR observation model

In this section, we first describe the linear mathematical model of the SAR observation process and then discuss the influence of phase errors on the observation model.

2.1 Observation model of a SAR imaging system

Here, imaging a scene of radius L in spotlight mode of SAR is considered. In spotlight mode, the platform moves in the azimuth direction and the squint angle θ varies by aperture position. In SAR systems, the transmitted signal is often a chirp signal as follows:

$$s(t) = \begin{cases} \exp(j(\omega_0 t + ht^2)) & |t| \le \frac{T_p}{2} \\ 0 & \text{otherwise} \end{cases} \tag{1}$$

where ω_0 is the carrier frequency and $2h$ is the chirp rate of the transmitted signal. This signal is transmitted to the scene to be imaged, and the received signal is mixed with the reference chirp signal and passed through a low-pass filter to produce the demodulated signal given by [3,7]:

$$r_\theta(t) = \iint_{x^2+y^2 \le L^2} f(x, y) \times \exp(-j\Omega(t)(x\cos\theta + y\sin\theta))\mathrm{d}x\mathrm{d}y \tag{2}$$

where L, $f(x, y)$, $\Omega(t) = \frac{2}{c}(\omega_0 t + 2h(t-\tau_0))$ and τ_0 denote the radius of the scene, the underlying field, radial spatial frequency, and demodulation time, respectively.

The demodulated signal is then sampled in all squint angles, so the discrete form of demodulated received signal for all azimuth positions, i.e., the phase history, becomes [3,7]:

$$\begin{bmatrix} \mathbf{r}_1 \\ \mathbf{r}_2 \\ \vdots \\ \mathbf{r}_P \end{bmatrix} = \begin{bmatrix} \mathbf{C}_1 \\ \mathbf{C}_2 \\ \vdots \\ \mathbf{C}_P \end{bmatrix} \mathbf{f} \Rightarrow \mathbf{r} = \mathbf{C}\mathbf{f} \tag{3}$$

where $\mathbf{r}$, $\mathbf{r}_i$ and $\mathbf{C}_i$ are the phase histories, discretized demodulated signal at the ith aperture position, and discrete approximation of the observation kernel in (2), respectively. The reflection coefficients of the field are stacked in the column vector $\mathbf{f}$. In a noisy environment, denoting the observation vector by $\mathbf{g}$ and the additive white Gaussian noise by $\mathbf{w}$, the linear observation model of a SAR system can be written as:

$$\mathbf{g} = \mathbf{C}\mathbf{f} + \mathbf{w} \tag{4}$$

2.2 Phase error and its influence on the observation model

According to relations (2) and (4) the discretized approximation of the observation kernel depends on the demodulation time. Perfect measurement of the demodulation time is impossible due to slip and mobility of the platform and atmospheric effects. Uncertainties in the position of the platform are assumed constant over a signal received at a particular aperture position, but vary across different aperture positions. Phase errors caused by such uncertainties are a function of the aperture position only.

Modeling such errors in the linear observation model is accomplished through the following procedure [6]. Denoting the demodulated signal vector in ith azimuth position in the presence of phase errors by $\mathbf{r}_{i_\varepsilon}$ and the error-free signal vector in the i-th azimuth position by $\mathbf{r}_i$, their relation can be expressed as:

$$\mathbf{r}_{i_\varepsilon} = e^{j\varphi_i}\mathbf{r}_i \quad i = 1, 2, \ldots, P \tag{5}$$

where φ_i is the phase error in the ith azimuth position. According to (5), all phase history elements can be stacked in a matrix form as:

$$\mathbf{r}_\varepsilon = \begin{bmatrix} \mathbf{K}_1 & 0 & \cdots & 0 \\ 0 & \mathbf{K}_2 & \ddots & \vdots \\ \vdots & \ddots & \ddots & 0 \\ 0 & \cdots & 0 & \mathbf{K}_P \end{bmatrix} \mathbf{r} \Rightarrow \mathbf{r}_\varepsilon = \mathbf{D}\mathbf{r} \tag{6}$$

where

$$\mathbf{K}_i = \begin{bmatrix} e^{j\varphi_i} & 0 & \cdots & 0 \\ 0 & e^{j\varphi_i} & \ddots & \vdots \\ \vdots & \ddots & \ddots & 0 \\ 0 & \cdots & 0 & e^{j\varphi_i} \end{bmatrix}_{Q\times Q} \tag{7}$$

that shows the phase error in the azimuth point i over all range positions. In (6), $\mathbf{D}$ is a diagonal matrix with size of $PQ \times PQ$ where P and Q are numbers of azimuth and range samples, respectively. Hence, the linear observation model in the presence of phase errors becomes:

$$\mathbf{g}_\varepsilon = \mathbf{DCf} + \mathbf{w} \tag{8}$$

where $\mathbf{g}_\varepsilon$ is the noisy phase-corrupted observation.

3 Proposed dictionary-based sparsity-driven autofocus algorithm

Sparsity-driven autofocus (SDA) algorithm proposed in [6], is an approach developed for joint SAR imaging and phase error correction through a nonquadratic regularization framework, assuming sparsity of the underlying scene. The proposed method of this paper provides an important extension over the SDA approach and facilitates sparsity-driven autofocusing on any scene containing any type of features. This is done by extending the sparse representation-based SAR imaging method [10] to the problem of joint SAR image formation and autofocus. This method can be used for any scene that has a sparse representation in terms of any signal dictionary, which includes scenes with piecewise smooth reflectivities, where the method in [6] may produce poor reconstructions.

Selection of a dictionary that can sparsify any wide area SAR image is still a challenging issue. However, there are some efforts in this regard. For example the work in [10] concluded that for SAR images of natural scenes the wavelet dictionary seems to be a good choice. Previous pieces of work have also established that the wavelet transform can sparsely represent natural scene images [11,12].

We have used small patches of SAR data involving highly spatially correlated areas for our experiments. For such real scenes, wavelet coefficients have a small number of nonzero high-frequency terms, and therefore the wavelet dictionary can sparsify this type of data. While we demonstrate the performance of our proposed approach with certain dictionaries in this paper, we do not necessarily claim that we have identified the best dictionary. However, we do believe that due to the spatially correlated nature of SAR reflectivities (although the structure of the correlation might be different from, e.g., optical images), there is certainly a need to consider sparse representations in various dictionaries. Accordingly, there is a need to develop autofocusing algorithms that can be used within the framework of such dictionary-based sparsity-driven image formation methods. This requires the kind of technical development presented in this paper. In that sense, this is a technical methodology paper whose goal is to make such a joint image formation and autofocusing algorithm available to radar imaging researchers and practitioners. Our framework and algorithm can be seamlessly used with any arbitrary dictionary.

In this method, we sparsely represent the magnitude of the complex-valued reflectivity field using a proper dictionary and estimate the sparse representation coefficients, unknown phase of reflectivity field, and the phase error vector by optimizing a multivariate cost function. The multivariate optimization we pose can be solved using a block coordinate descent approach. The first subsection below describes the dictionary-based sparse representation and autofocus framework we propose. The second subsection contains the details of the iterative algorithm we develop for solving the optimization problem posed.

3.1 Dictionary-based sparse representation framework

Considering the complex-valued nature of the SAR image, the reflectivity field can be expressed as follows:

$$\mathbf{f} = \Phi|\mathbf{f}| \tag{9}$$

In this equation $\Phi = \text{diag}\{e^{j\beta_l}\}$ where β_l is the phase of lth component of vector $\mathbf{f}$ and $|\mathbf{f}|$ is the magnitude of the vector $\mathbf{f}$.

Since features of the magnitude of the reflectivity field are usually important [10], the new dictionary-based approach is designed to sparsely represent the magnitude of the image as:

$$|\mathbf{f}| = \Psi\mathbf{a} \tag{10}$$

where Ψ is an appropriate dictionary that sparsely represents magnitude of the complex-valued image and $\mathbf{a}$ denotes the

sparse representation coefficients. Now we substitute (9) and (10) into the observation model (8):

$$\begin{aligned}\mathbf{g}_\varepsilon &= \mathbf{DCf} + \mathbf{w} = \mathbf{DC}\Phi|\mathbf{f}| + \mathbf{w} = \mathbf{DC}\Phi\Psi\mathbf{a} + \mathbf{w} \\ &= \text{diag}\{\mathbf{d}\}\ \mathbf{C}\ \text{diag}\{\mathbf{b}\}\ \Psi\mathbf{a} + \mathbf{w} \end{aligned} \tag{11}$$

In (11) $\mathbf{b}$ is a vector with elements $(\mathbf{b})_l = e^{j\beta_l}$. Also, $\mathbf{d}$ is a vector with elements $(\mathbf{d})_i = e^{j\varphi_i}$ where φ_i is the i-th element of the phase error vector.

What we propose is a combined algorithm for complex-valued SAR imaging that finds both the magnitude and the phase of the reflectivities, where we incorporate prior information about the magnitude field through sparse representation and assume no prior information on the phase field (so we essentially perform maximum likelihood estimation on phase, but if any such information is available, it can in principle be included in our approach through extra terms involving the phase). As a cartoon example, think of a complex-valued scene $\mathbf{f}$ with piecewise constant (or smooth) reflectivity magnitudes and random, uniformly distributed phase. The magnitude of such a scene would admit sparse representation, whereas its real and imaginary parts would not. So if we tried to linearly represent such an $\mathbf{f}$ through a dictionary, that would amount to trying to represent the real and imaginary parts sparsely, which would not work due to the random-phase nature of SAR.

We want to reconstruct the sparse coefficients $\mathbf{a}$, which defines the magnitude image $|\mathbf{f}|$, from noisy observations $\mathbf{g}_\varepsilon$, in the presence of the unknown phase matrix and the phase error matrix $\mathbf{D}$. This problem can be solved through the following optimization problem.

$$\begin{aligned}\{\hat{\mathbf{d}}, \hat{\mathbf{b}}, \hat{\mathbf{a}}\} = \underset{\mathbf{d},\mathbf{b},\mathbf{a}}{\text{argmin}} &(\|\mathbf{g}_\varepsilon - \text{diag}\{\mathbf{d}\}\ \mathbf{C}\ \text{diag}\{\mathbf{b}\}\ \Psi\mathbf{a}\|_2^2 \\ &+ \lambda\|\mathbf{a}\|_p^p + \lambda'\left(\sum_{l=1}^{I}(|(\mathbf{b})_l|^q - 1)^2\right) \\ &+ \lambda''\left(\sum_{i=1}^{PQ}(|(\mathbf{d})_i|^u - 1)^2\right)\end{aligned} \tag{12}$$

where I is the total number of elements of $\mathbf{b}$.

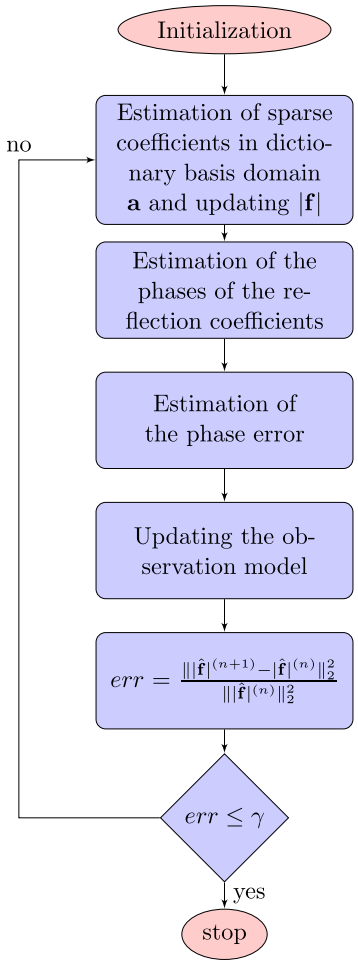

This multivariate nonlinear estimation problem can be solved using three linear problems in a block coordinate descent scheme. This optimization problem is generally not convex, so there is no guarantee for convergence of the algorithm to the global minimum; however, we usually get a good solution (at a local minimum) starting from a reasonable initialization (e.g., a conventional reconstruction). The iterative algorithm of dictionary-based sparsity-driven autofocus (DBSDA), which we develop with this perspective, is sketched as the above flowchart.

3.2 The DBSDA algorithm

According to the observation model in (11) and overall optimization problem in (12), if Φ and $\mathbf{D}$ were known, an estimate of $\mathbf{a}$ and hence the image itself could be found using an atomic decomposition technique [13] such as an extension of basis pursuit as [14]:

$$\hat{\mathbf{a}} = \underset{\mathbf{a}}{\operatorname{argmin}} \parallel \mathbf{g}_\varepsilon - \mathbf{DC}\Phi\Psi\mathbf{a} \parallel_2^2 + \lambda \parallel \mathbf{a} \parallel_p^p \tag{13}$$

where $\| \cdot \|_p$ denotes the l_p norm and λ is a regularization parameter. The first term in (13) is a data fidelity term, and the second term uses $p \leqslant 1$ to enforce sparsity of the representation [15,16].

However, image vector element phases and elements of the phase error matrix are unknown. In order to overcome this problem, the following coordinate descent algorithm is proposed.

3.2.1 Initialization

In this step, the image formed by the conventional polar format algorithm (PFA) is used to initialize the algorithm. Then initial estimate of the phase matrix can be produced based on the phases of the PFA image. Initial value of phase error is considered to be 0 for all azimuth positions and so the initial value of $\mathbf{D}$ is set to the identity matrix, i.e., $\mathbf{D} = \mathbf{I}$.

3.2.2 Estimation of $\mathbf{a}$

In this step, the optimization problem in (13) can be solved using the initial estimates of $\mathbf{D}$ and Φ matrices. In order to avoid problems due to nondifferentiability of the l_p norm, a smooth approximation is used as [7]:

$$\| \mathbf{a} \|_p^p \approx \sum_{i=1}^{I} (| (\mathbf{a})_i |^2 + \eta)^{\frac{p}{2}} \tag{14}$$

where I and η are the total number of elements of $\mathbf{f}$ and a nonnegative small constant, respectively. With the slight modification in (14), the cost function in (13) becomes:

$$\begin{aligned} J(\mathbf{a}) = {} & \mathbf{g}_\varepsilon^H \mathbf{g}_\varepsilon - \mathbf{g}_\varepsilon^H (\mathbf{DC}\Phi\Psi)\mathbf{a} - \mathbf{a}^H (\mathbf{DC}\Phi\Psi)^H \mathbf{g}_\varepsilon \\ & + \mathbf{a}^H (\mathbf{DC}\Phi\Psi)^H (\mathbf{DC}\Phi\Psi)\mathbf{a} + \lambda \sum_{i=1}^{I} \left(| (\mathbf{a})_i |^2 + \eta \right)^{\frac{p}{2}} \end{aligned} \tag{15}$$

Gradient of the cost function with respect to $\mathbf{a}$ becomes:

$$\nabla_a J(\mathbf{a}) = M(\mathbf{a})\mathbf{a} - 2(\mathbf{DC}\Phi\Psi)^H \mathbf{g}_\varepsilon \tag{16}$$

where

$$M(\mathbf{a})\mathbf{a} = 2(\mathbf{DC}\Phi\Psi)^H (\mathbf{DC}\Phi\Psi) + \lambda p \Gamma(\mathbf{a}) \tag{17}$$

and

$$\Gamma(\mathbf{a}) = \operatorname{diag} \left\{ \frac{1}{(|(\mathbf{a})_i|^2 + \eta)^{1-\frac{p}{2}}} \right\} \tag{18}$$

This optimization problem has no closed-form solution. Here we use a quasi-Newton method with a particular Hessian update scheme [17]:

$$\hat{\mathbf{a}}^{(n+1)} = \hat{\mathbf{a}}^{(n)} - \rho [M(\hat{\mathbf{a}}^{(n)})]^{-1} \nabla_a J(\mathbf{a}) \tag{19}$$

where $M(\mathbf{a})$ is an approximation of the Hessian. The step size is assumed to be $\rho = 1$ which guarantees the convergence of the algorithm. Substituting (16), (17) and (18) in (19), we can find an estimate of $\mathbf{a}$ through:

$$\begin{aligned} \hat{\mathbf{a}}^{(n+1)} = {} & (2(\mathbf{DC}\Phi\Psi)^H (\mathbf{DC}\Phi\Psi) \\ & + \lambda p \Gamma(\hat{\mathbf{a}}^{(n)}))^{-1} (2(\mathbf{DC}\Phi\Psi)^H \mathbf{g}_\varepsilon) \end{aligned} \tag{20}$$

Evaluating the matrix inversion term of the right side in (16) is not efficient, and therefore the equivalent linear form of this equation is solved instead, using the conjugate gradient (CG) method [18,19].

The quasi-Newton method and the CG are serving two different objectives. The outer iteration in our algorithm can be interpreted as a quasi-Newton method (another interpretation is what is called half-quadratic regularization). Each iteration of that algorithm requires solution of a set of linear equations. This is where we use a set of inner CG iterations.

The algorithm begins with an initial estimate of $\mathbf{a}$ and runs until it converges. Then, a new estimate of $|\mathbf{f}|$ can be obtained according to (11).

"Although we seek a sparse representation of $|\mathbf{f}| = \Psi\mathbf{a}$, we do not check whether the representation obtained from the above algorithm always yields a positive-valued signal. This causes an extra redundancy in our model insofar as a negative magnitude can be compensated by a phase shift of π. One could try and limit the approach to guarantee positive numbers in the magnitude representation, and however, that would lead to additional computational complexity. In our work, we have not felt the need to limit the solution to be nonnegative [10]".

3.2.3 Estimation of the phase of the complex-valued image

Estimating the phase matrix of the complex-valued image requires the observation model to be expressed slightly differently. The diagonal components of matrix Φ are placed in the vector $\mathbf{b}$, and the elements of $|\mathbf{f}|$ from the previous step,

are placed in diagonal components of a diagonal matrix $\mathbf{H}$, i.e., $\mathbf{H} = \text{diag}\{|\mathbf{f}_i|\}$. Hence, the modified observation model becomes:

$$\mathbf{g}_\varepsilon = \mathbf{DCHb} + \mathbf{w} \tag{21}$$

We can find an estimate of $\mathbf{b}$ through the following optimization problem:

$$\hat{\mathbf{b}} = \underset{\mathbf{b}}{\text{argmin}} \, \|\mathbf{g}_\varepsilon - \mathbf{DCHb}\|_2^2 + \lambda' \|\mathbf{b}\|_{2q}^{2q} - 2\lambda' \|\mathbf{b}\|_q^q \tag{22}$$

The details of the derivation of Eq. (22) which is a MAP estimator of $\mathbf{b}$ can be found in the electronic supplementary material. This problem can be solved using the same type of quasi-Newton scheme previously used for $\mathbf{a}$:

$$\acute{T}(\hat{\mathbf{b}}^{(n)})\hat{\mathbf{b}}^{(n+1)} = 2(\mathbf{DCH})^H \mathbf{g}_\varepsilon \tag{23}$$

where

$$\acute{T}(\hat{\mathbf{b}}^{(n)}) = 2(\mathbf{DCH})^H(\mathbf{DCH}) + 2\lambda' q \Gamma_1(\hat{\mathbf{b}}^{(n)}) - 2\lambda' q \Gamma_2(\hat{\mathbf{b}}^{(n)}) \tag{24}$$

and

$$\Gamma_1(\mathbf{b}) = \text{diag}\left\{\frac{1}{(|\mathbf{b}_i|^2 + \eta)^{1-q}}\right\}, \quad \Gamma_2(\mathbf{b}) = \text{diag}\left\{\frac{1}{(|\mathbf{b}_i|^2 + \eta)^{1-\frac{q}{2}}}\right\} \tag{25}$$

Equation (23) can be solved using the CG method. The iterative algorithm for solving (23) must be run until

$$\left(\frac{\|\hat{\mathbf{b}}^{(n+1)} - \hat{\mathbf{b}}^{(n)}\|_2^2}{\|\hat{\mathbf{b}}^{(n)}\|_2^2}\right) \leq \delta_{\mathbf{b}} \tag{26}$$

where $\delta_{\mathbf{b}}$ is a small positive real constant. The estimate of Φ is then given by:

$$\Phi = \text{diag}\{\mathbf{b}\} \tag{27}$$

3.2.4 Estimation of the phase error components

In previous steps of the DBSDA algorithm, we have estimated the phase matrix Φ, and the magnitude vector $|\mathbf{f}|$. Using these estimated variables and (10) the complex-valued reflectivity vector is estimated. Then the phase history vector $\mathbf{r}$ is estimated using (3). The observation model in (9) can be written as:

$$\mathbf{g}_\varepsilon = \mathbf{DCf} + \mathbf{w} = \mathbf{Dr} + \mathbf{w} \tag{28}$$

Denoting the diagonal matrix $\mathbf{R} = \text{diag}\{\mathbf{r}\}$, and the vector formed by stacking the diagonal elements of matrix $\mathbf{D}$ by $\mathbf{d}$, the observation model can be put into the following form:

$$\mathbf{g}_\varepsilon = \mathbf{Dr} + \mathbf{w} = \mathbf{Rd} + \mathbf{w} \tag{29}$$

Assuming phase error in each azimuth position independent from other azimuth positions with uniform pdf, we can introduce the MAP estimator of $\mathbf{d}$ as follows:

$$\hat{\mathbf{d}} = \underset{\mathbf{d}}{\text{argmin}} \, \|\mathbf{g}_\varepsilon - \mathbf{Rd}\|_2^2 + \lambda'' \|\mathbf{d}\|_{2u}^{2u} - 2\lambda'' \|\mathbf{d}\|_u^u \tag{30}$$

The details of the derivation of Eq. (30) can be found in the electronic supplementary material. This problem can be solved using a similar quasi-Newton scheme previously used for $\mathbf{b}$:

$$[2(\mathbf{R})^H(\mathbf{R}) + 2\lambda'' u \Gamma_1(\hat{\mathbf{d}}^{(n)}) - 2\lambda'' u \Gamma_2(\hat{\mathbf{d}}^{(n)})]\hat{\mathbf{d}}^{(n+1)} = 2\mathbf{R}^H \mathbf{g}_\varepsilon \tag{31}$$

We use conjugate gradient algorithm to solve (31). This algorithm runs until:

$$\left(\frac{\|\hat{\mathbf{d}}^{(n+1)} - \hat{\mathbf{d}}^{(n)}\|_2^2}{\|\hat{\mathbf{d}}^{(n)}\|_2^2}\right) \leq \delta_{\mathbf{d}} \tag{32}$$

where $\delta_{\mathbf{d}}$ is a small positive constant.

Although for the sake of generality we have assumed 2D phase errors, the majority of phase errors (e.g., those due to platform location uncertainties) are 1D functions of the azimuth position. It can be easily shown that this additional constraint results in the closed-form solution given in [6].

3.2.5 Updating the observation model

After estimation of $\mathbf{d}$, the matrix $\mathbf{D} = \text{diag}\{\mathbf{d}\}$, needs to be updated in each iteration.

Obtaining the updated matrix $\mathbf{D}$, we can go back to step 2 of the algorithm (estimation of $\mathbf{a}$). This iterative scheme runs until the image is formed and phase error is estimated and compensated according to the algorithm stopping criteria. Penalty parameter selection affects the quality of the reconstructed image.

Parameter selection is a common concern in many optimization problems, including sparse representation problems. There is a separate body of work on automatic parameter choice [20]. One can certainly employ one of these parameter choice techniques when using our approach, but that is beyond the scope of the current paper. Convergence of the algorithm in terms of cost functional can be easily established in a similar way to that in [10].

Table 1 SAR system parameter

Carrier frequency (ω_0)	$2\pi \times 10^{10}$ $\frac{\text{rad}}{\text{s}}$
Chirp rate (2 h)	$2\pi \times 10^{12}$ $\frac{\text{rad}}{\text{s}^2}$
Puls duration (T_p)	4×10^{-4} s
Range and azimuth resolution (δ_r, δ_{az})	0.375 m

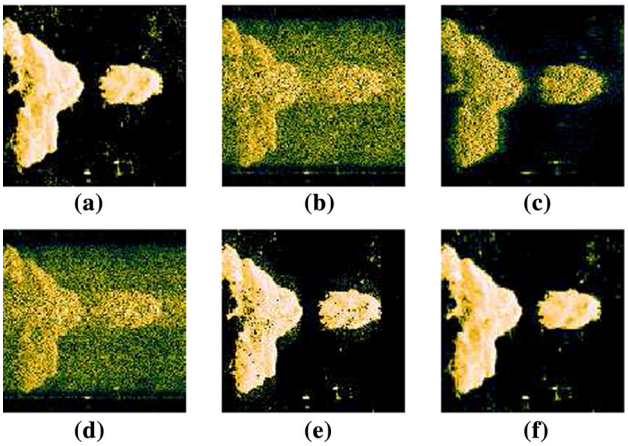

Fig. 1 Reconstruction of a SAR data extracted from a real SIR-C/X-SAR image in the presence of phase errors. **a** Reference underlying scene, **b** conventional PFA reconstruction, **c** PFA + PGA autofocus method, **d** PFA + MCA autofocus method, **e** SDA method, **f** the DBSDA method

4 Experimental results

We present experimental results using synthetic and real SAR images. The dictionary used in this paper consists of wavelet atoms. We compare the results of DBSDA to PGA, MCA, and SDA. This comparison demonstrates the potential of our algorithm to produce better results, which is obtained at the cost of increased computational complexity. For generation of synthetic SAR phase history data, we have used the system parameters shown in Table 1.

In the first experiment, the aim is to test the performance of the proposed algorithm on a synthetic image with a large smooth region. Results of this experiment is shown in the electronic supplementary material.

In the next experiment, we apply different reconstruction methods on data extracted from a real SIR-C/X-SAR image of 128 × 128 pixels [21]. We have generated the raw data using the observation model in (4) (or (8) in the presence of the phase errors) from the complex SAR image. Figure 1a shows the reference underlying scene. Figure 1b–f shows the reconstructed images using conventional reconstruction and different autofocus methods. Phase errors are random with uniform distribution in the interval $[-\frac{\pi}{2}, \frac{\pi}{2}]$. The SNR is 20dB.

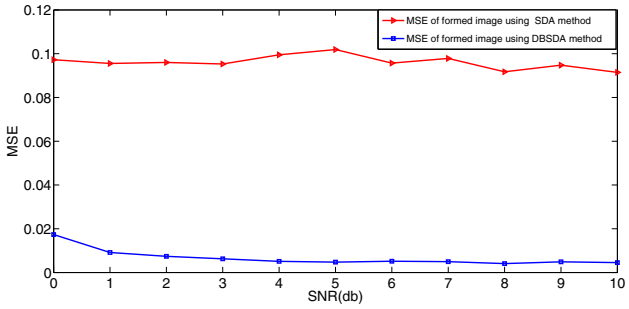

Fig. 2 Mean squared error of the reconstructed image in Fig. 1 using SDA and DBSDA methods

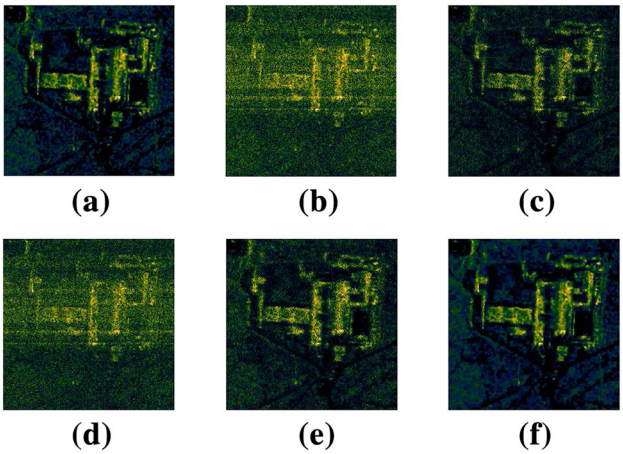

Fig. 3 Reconstruction of real TerraSAR-X data in the presence of phase error. **a** Reference underlying scene, **b** conventional PFA reconstruction, **c** PFA + PGA autofocus method, **d** PFA + MCA autofocus method, **e** SDA method, **f** DBSDA method

The figures of real and estimated phase errors using SDA and DBSDA methods for all azimuth positions, as well as the error of phase error estimation can be found in electronic supplementary material. They show that in most azimuth positions DBSDA method can achieve better phase error estimation in comparison with the SDA method.

Finally, the mean squared error of the reconstructed image versus different signal to noise ratios is shown in Fig. 2 for this experiment, using SDA and DBSDA. These results show that DBSDA is more effective, in simultaneous image formation and phase error estimation and compensation, than SDA for SAR scenes composed of piecewise smooth reflectivities.

In the last experiment we apply different reconstruction and autofocus methods on a real patch of TerraSAR-X data of 256 × 256 pixels. We have used the reverse bi-orthogonal wavelet (rbio1.1) dictionary DBSDA. Figure 3b–f shows the reconstructed images using conventional reconstruction and different autofocus methods. In this simulation the SNR is 25 dB. Results in Fig. 3 demonstrate that DBSDA outperforms other autofocusing techniques. Also Fig. 4 shows the mean squared error versus SNR of the reconstructed image

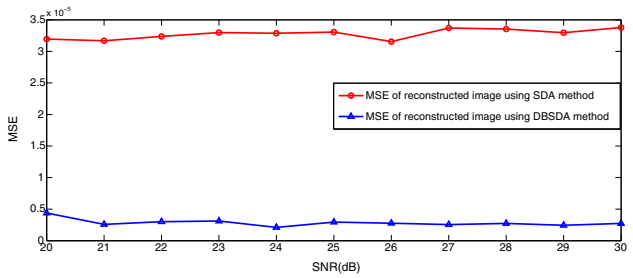

Fig. 4 Mean squared error of the reconstructed TerraSAR-X image using SDA and DBSDA methods

Table 2 The run times of different techniques (s)

Techniques	1st Exp	2nd Exp	3rd Exp
PFA + PGA	0.076488	0.837312	4.332716
PFA + MCA	0.088197	0.386849	2.605853
SDA	5.474754	5.067594	42.89076
DBSDA	7.462061	11.36453	48.10363

for DBSDA and SDA. This result shows that DBSDA provides much lower mean squared errors than SDA. We have calculated the run times of different autofocus techniques in all experiments carried on an Intel core i5 2.5 GHz processor. These results are depicted in Table 2. Overall, our experiments show the ability of the proposed DBSDA algorithm to produce better results, obtained at the cost of more computational complexity.

5 Conclusion

In this paper, we have introduced a novel simultaneous SAR image formation and autofocusing technique. Our algorithm extends the idea of exploiting sparsity in the autofocusing process [6] from scenes that are directly sparse in the image domain to scenes that admit sparse representation in terms of any dictionary. To this end, we pose a sparsity-driven optimization problem through which we estimate and compensate the phase errors by a block coordinate descent algorithm in the image formation process. Experimental results with synthetic and real SAR images show that the DBSDA algorithm offers better performance than both the post-processing-based autofocus algorithms and the SDA method in reconstruction of scenes that are not directly sparse in the image domain. The quantitative MSE measure of the quality is also evaluated and supports this observation. Also for further analysis, the abilities of SDA and DBSDA to correctly estimate the unknown phase errors are investigated, which shows that DBSDA outperforms SDA for a scene with piecewise smooth reflectivities.

References

1. Wiley, C.A.: Pulsed Doppler radar methods and apparatus. Google Patents (1965)
2. Jakowatz, C.V., Wahl, D.E., Eichel, P.H., Ghiglia, D.C., Thompson, P.A.: Spotlight-Mode Synthetic Aperture Radar: A Signal Processing Approach, vol. 101. Kluwer, Norwell (1996)
3. Carrara, W.G., Goodman, R.S., Majewski, R.M.: Spotlight Synthetic Aperture Radar: Signal Processing Algorithms. Artech House, Boston (1995)
4. Wahl, D., Eichel, P., Ghiglia, D., Jakowatz Jr., C.: Phase gradient autofocus—a robust tool for high resolution SAR phase correction. IEEE Trans. Aerosp. Electron. Syst. **30**, 827–835 (1994)
5. Morrison, R.L., Do, M.N., Munson, D.C.: MCA: a multichannel approach to SAR autofocus. IEEE Trans. Image Process. **18**, 840–853 (2009)
6. Önhon, N.Ö., Çetin, M.: A sparsity-driven approach for joint SAR imaging and phase error correction. IEEE Trans. Image Process. **21**, 2075–2088 (2012)
7. Çetin, M., Karl, W.C.: Feature-enhanced synthetic aperture radar image formation based on nonquadratic regularization. IEEE Trans. Image Process. **10**, 623–631 (2001)
8. Kelly, S., Yaghoobi, M., Davies, M.: Sparsity-based autofocus for undersampled synthetic aperture radar. IEEE Trans. Aerosp. Electron. Syst. **50**, 972–986 (2014)
9. Ügur, S., Arkan, O.: SAR image reconstruction and autofocus by compressed sensing. Digit. Signal Process. **22**(6), 923–932 (2012)
10. Samadi, S., Çetin, M., Masnadi-Shirazi, M.A.: Sparse representation-based synthetic aperture radar imaging. IET Radar Sonar Navig. **5**, 182–193 (2011)
11. Starck, J.L., Elad, M., Donoho, D.L.: Image decomposition via the combination of sparse representations and a variational approach. IEEE Trans. Image Process. **14**(10), 1570–1582 (2005)
12. Donoho, D.L., Johnstone, I.: Ideal spatial adaptation via wavelet shrinkage. Biometrika **81**, 425–455 (1994)
13. Chen, S.S., Donoho, D.L., Saunders, M.A.: Atomic decomposition by basis pursuit. SIAM J. Sci. Comput. **20**, 33–61 (1998)
14. Samadi, S., Çetin, M., Masnadi-Shirazi, M.A. :Sparse signal representation for complex-valued imaging. In: 13th IEEE Digital Signal Processing Workshop, pp. 365–370 (2009)
15. Elad, M., Bruckstein, A.M.: A generalized uncertainty principle and sparse representation in pairs of bases. IEEE Trans. Inf. Theory **48**, 2558–2567 (2002)
16. Malioutov, D.M., Çetin, M., Willsky, A.S.: Optimal sparse representations in general overcomplete bases. In: IEEE International Conference on Acoustics, Speech, and Signal Processing, (ICASSP'04), pp. ii-793-6 (2004)
17. Bonnans, J.F., Gilbert, J.C., Lemarechal, C., Sagastizabal, C.A.: Numerical Optimization: Theoretical and Practical Aspects. Springer, Berlin (2006)
18. Golub, G.H., Van Loan, C.F.: Matrix Computations. JHU Press, Baltimore (2012)
19. Çetin, M., Karl, W.C., Willsky, A.S.: Feature-preserving regularization method for complex-valued inverse problems with application to coherent imaging. Opt. Eng. **45**, 017003-11 (2006)
20. Batu, O., Çetin, M.: Parameter selection in sparsity-driven SAR imaging. IEEE Trans. Aerosp. Electron. Syst. **47**(4), 3040–3050 (2011)
21. http://photojournal.jpl.nasa.gov/catalog/pia01843